The Journal of Chemical Physics

Classical coherent two-dimensional vibrational spectroscopy

Cite as: J. Chem. Phys. **148**, 064101 (2018); https://doi.org/10.1063/1.5017985
Submitted: 01 December 2017 • Accepted: 19 January 2018 • Published Online: 08 February 2018

Mike Reppert and Paul Brumer

Classical coherent two-dimensional vibrational spectroscopy

Mike Reppert[1,a)] and Paul Brumer[2]
[1]*Chemical Physics Theory Group, Department of Chemistry, University of Toronto, Toronto, Ontario M5S 3H6, Canada*
[2]*Chemical Physics Theory Group, Department of Chemistry, and Center for Quantum Information and Quantum Control, University of Toronto, Toronto, Ontario M5S 3H6, Canada*

(Received 1 December 2017; accepted 19 January 2018; published online 8 February 2018)

Two-dimensional (2D) ultrafast spectroscopy is a powerful tool for studying the electronic and vibrational structures of complex systems. Unfortunately, the physical interpretation of these experiments is obscured by conceptual problems in classical response theory, i.e., the divergence of classical nonlinear response functions. We demonstrate that these difficulties are avoided by modeling classical 2D experiments nonperturbatively, illustrating that nonlinear spectroscopy and nonlinear response are not synonymous. Numerical simulations allow a direct comparison between classical and quantum 2D spectra for simple, weakly anharmonic systems relevant to vibrational spectroscopy. We find that nonperturbative classical theory—although differing in quantitative details—accurately captures the key qualitative features of the quantum 2D spectrum, including the separation of the signal into wavevector-selected pathways, formation of cross peaks between coupled vibrational modes, and coherent beating in the signal as a function of waiting time (so-called "quantum beats"). These results are discussed in terms of a simple analytical model which captures the key physical features of classical 2D spectroscopy and provides a link between classical and quantum descriptions. One interesting conclusion from this comparison is that the "coherence" observed in ultrafast spectroscopy may (at least in vibrational experiments) be understood as a purely classical phenomenon, without reference to quantum mechanics. *Published by AIP Publishing.* https://doi.org/10.1063/1.5017985

I. INTRODUCTION

In recent years, the fields of optical and infrared (IR) multidimensional spectroscopy have seen tremendous technical developments and a rapidly expanding range of applications in physics, chemistry, and biology. As natural extensions of multidimensional nuclear magnetic resonance (NMR) experiments to the visible and infrared (IR) regimes, these ultrafast laser-based techniques offer detailed views into molecular and electronic processes on time scales that had until recently been outside of the range of experimental measurement.[1] In the visible frequency range, two-dimensional electronic spectroscopy (2D ES) offers a glimpse into the ultrafast energy- and electron-transfer processes in biological light harvesting proteins and in artificial solar cells.[2,3] In the vibrational regime, two-dimensional infrared (2D IR) spectroscopy probes the rapid structural rearrangements of complex molecular systems such as proteins, nucleic acids, and even water.[4,5]

Despite these successes, the interpretation of experimental 2D spectra remains, in many cases, a difficult task. Nowhere has this difficulty been so apparent as in the recent discussion of coherent beating signals observed in 2D ES experiments on natural light-harvesting proteins.[6–9] Interpreted within a quantum-mechanical framework, these signals correspond to coherent superpositions of system eigenstates and were initially interpreted as evidence that quantum coherence may be important in biological light harvesting.[6,8,10] Later interpretations, however, attributed the beating signals to coherent vibrational or vibronic—rather than strictly electronic—dynamics.[11–13] It has also been emphasized that coherent population dynamics are unlikely to persist under the incoherent solar radiation that excites biological pigments in their natural environment.[14,15] Finally, several authors have noted that similar coherent oscillations can occur in analogous classical and semiclassical systems and may thus not be an exclusively quantum effect.[16–19] From an essentially uncontroversial set of experimental data has thus emerged a controversial discussion of physical significance.

Aside from the inherent challenge of disentangling nuclear and electronic dynamics, the difficulty in interpreting 2D spectra stems in part from conceptual problems in classical nonlinear response. In contrast to the relatively clean analogy between quantum and classical linear response (e.g., absorption), quantum-classical correspondence in nonlinear processes is complex.[20] In fact, as demonstrated by Kryvohuz and Cao, classical nonlinear response functions—core ingredients in the standard perturbative framework for nonlinear spectroscopy—are generally unstable, diverging toward infinity at long times.[21] In the absence of a simple classical description, quantum-mechanical concepts have become firmly embedded in the language of 2D spectroscopy, e.g., the ubiquitous density-matrix descriptors "coherence" and "population." Significantly, this reliance on quantum terminology extends even to nonlinear vibrational spectroscopy, which one might expect to be well-described classically. In

a)mreppert@alum.mit.edu

this context, it is perhaps not surprising that oscillatory signals ("quantum beats") have a tendency to be automatically associated with quantum-mechanical effects.

The purpose of this contribution is two-fold. First, we demonstrate through nonperturbative numerical simulations—beyond the nonlinear response framework—that, for weakly anharmonic systems, 2D spectroscopies admit of a well-defined, conceptually oriented classical description that in its qualitative features closely resembles the familiar quantum results, including "quantum beats." Second, by means of a simple nonperturbative analytical model, we offer an intuitive explanation for the physical origins and significance of the classical divergence of spectroscopic response functions. Together these results offer significant insight into the physics of 2D spectroscopy.

II. NUMERICAL RESULTS

A. 2D spectroscopy without response functions

For most ultrafast spectroscopists, a coherent 2D experiment is almost synonymous with the determination of a third-order response function. The generic instability of classical response functions[21] may thus be rather startling since it apparently suggests a manifestly unphysical divergence of signals for classical systems.

In fact, classical theory predicts no such unphysical behavior. The difficulty lies in the mathematical structure of the nonlinear response formalism, not in the underlying classical dynamics. To clarify this issue, we explore in this section a series of nonperturbative numerical simulations that illustrate the predictions of classical physics for nonlinear spectroscopy.

As a background, consider the essential physical features of coherent, time-domain, 2D spectroscopy. In a typical 2D experiment, a sample is subjected to a series of three ultrafast laser pulses, separated by delay times τ_1 and τ_2. At some time τ_3 after the arrival of the last pulse, the "response," i.e., macroscopic polarization, of the system is monitored indirectly via the emitted electromagnetic field.[22] By varying the control parameters that define each pulse (e.g., phase, amplitude, polarization, or propagation axis), the experimentalist isolates the portion of the response that depends on the control parameters for all three pulses or some Fourier sub-component of this signal. Signal components that depend on only one or two of the three pulses are either removed by direct subtraction or suppressed by experimental design. In a 2D measurement in the BOXCARS geometry, for example, one selects the signal whose wavevector-matched propagation axis is a particular sum or difference of the wavevectors of all three input pulses.[22]

Two-dimensional experiments are typically described using nonlinear response,[23] where the measured 2D signal corresponds (in the low-fluence, short-pulse limit) to the third-order response tensor. In classical theory, however, the nonlinear response expansion is unstable even for simple integrable systems. Fortunately, such systems are readily amenable to numerical simulations that avoid the nonlinear response framework by directly propagating the system dynamics in the presence of the perturbing electric fields. By a judicious combination of simulations, the relevant 2D signal can then be extracted from the total system response.

To be precise, denoted by $S^{[k]}$ is the signal generated with only the kth pulse present; likewise $S^{[jk]}$ is the signal generated by pulses j and k together, and $S^{[123]}$ is the signal generated by all three pulses. In any experiment, we may take by definition the component $S^{(k)}$ of the signal generated by pulse k as

$$S^{(k)} \equiv S^{[k]}. \tag{1}$$

Likewise, the signal component $S^{(jk)}$ that depends simultaneously on pulses j and k may be isolated as the difference

$$S^{(jk)} \equiv S^{[jk]} - S^{[j]} - S^{[k]}. \tag{2}$$

Similarly, to isolate the signal component that depends on all three pulses, we define

$$S^{(123)} \equiv S^{[123]} - S^{(1)} - S^{(2)} - S^{(3)} - S^{(12)} - S^{(13)} - S^{(23)} \tag{3}$$

removing from the total signal those components that are functions only of any individual pulse or pulse pair.

In case, a nonlinear response expansion is valid for the experiment, it is readily verified that the signal $S^{(123)}$ defined in this way corresponds, in the low-intensity limit, to the contribution of the third-order response function. Equation (3) is more general, however, since it is independent of any specific theoretical framework. For certain applications (e.g., all-collinear geometries), this definition may even be of use experimentally, although in most cases the automatic signal selection offered, for example, by wavevector matching will be much more efficient. Note that this is not the only convention possible for a 2D experiment; more complicated phase-cycling procedures could be devised, for example, to select specific Fourier components of the nonlinear signal. For present purposes, it suffices to separate Fourier components by direct time-domain filtering, as discussed in Sec. II B.[24]

B. Classical 2D spectra

Consider then the predictions of classical dynamics for 2D spectroscopy of a single Morse oscillator. For convenience, let the system parameters (harmonic frequency, anharmonicity, and dipole strength) be chosen to mimic the extensively studied Amide I (peptide carbonyl stretch) vibration. To evaluate the full nonlinear response, we classically propagate the oscillator coordinates (initially at rest) in the presence of various perturbing electromagnetic fields over a simulated scan time of T_{scan} = 3 ps.[25] For simplicity, the signal is calculated in the all-parallel (ZZZZ) polarization, with the laser field oriented parallel to the oscillator dipole.[26] The method is thus similar in spirit to the finite-field Raman calculations of Refs. 27–29 although no effort is made to isolate specific orders of response since nonlinear response functions for the Morse oscillator are known to diverge.[21] The 2D signal is calculated according to Eq. (3). After explicitly heterodyning the signal by interference with the final pulse amplitude, we Fourier transform along both τ_1 and τ_3 to obtain 2D spectra. A Dolph-Chebyshev window[30] with an attenuation of 100 dB is applied in the time domain to provide a finite line width in the frequency domain and to eliminate ringing artifacts in the numerical Fourier transform. Further details are provided in Appendix A.

Classical results for a 2D experiment with $\tau_2 = 0$ and a laser pulse power of 2 nJ are presented in frames (a), (c), and (e)

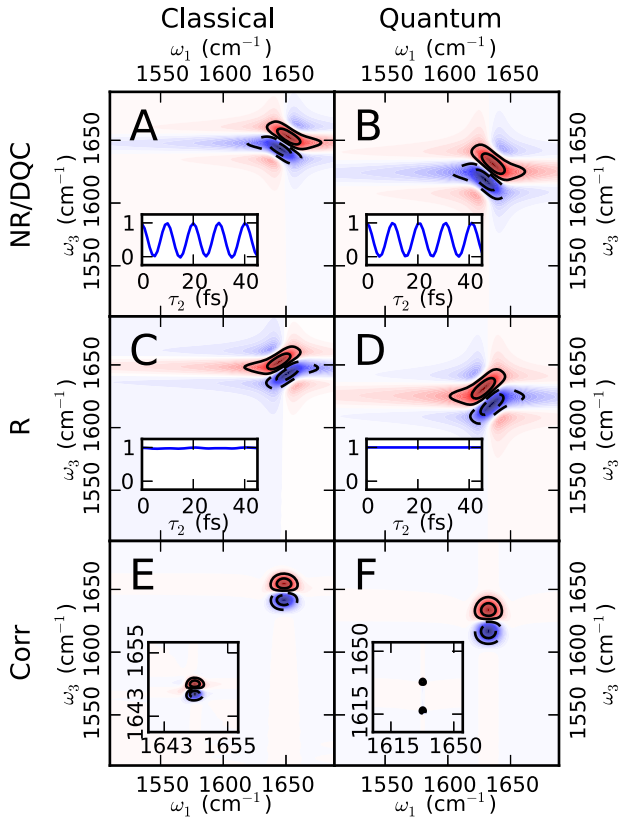

FIG. 1. 2D Spectra for a Morse oscillator according to classical dynamics [frames (a), (c), and (e)] or the third-order quantum response function [frames (b), (d), and (f)]. Frames (a) and (b) represent NR- and DQC-like components; frames (c) and (d) represent R-like components; and frames (e) and (f) represent the correlation spectrum. The red shading represents negative (bleach) features, while the blue shading represents positive features (induced absorption). The insets of frames (a)–(d) graph the depth of the bleach feature as a function of τ_2. The insets of frames (e) and (f) present the corresponding 2D spectra obtained for a longer scan time of T_{scan} = 20 ps (compared with T_{scan} = 3 ps in the main frame).

of Fig. 1. The corresponding quantum signals, as predicted by the third-order response function, are provided for comparison in frames (b), (d), and (f). As in the quantum case, the classical signal is separated into a nonrephasing/double-quantum coherence (NR/DQC) component characterized by the signals at positive frequencies in ω_1 [frames (a) and (b)] and a rephasing (R) component characterized by negative frequencies in ω_1 [frames (c) and (d)]. In accord with convention, the ω_1 axis for the rephasing pathway is inverted so as to plot all signals at positive frequencies. Panels (e) and (f) represent the correlation surfaces formed, as described below, by combining the rephasing and nonrephasing signals.

Comparison of the quantum and classical spectra reveals a close similarity in form, particularly the symmetry of the mixed absorptive/dispersive features, but differences in precise frequencies. This qualitative similarity is further emphasized in the τ_2-dependence of the signals. The inset plots in frames (a)–(d) graph as a function of τ_2 the depth of the bleaching feature (negative signal, red shading) at a fixed frequency corresponding to the maximum depth at $\tau_2 = 0$. (All signals are normalized to a maximum depth of 1.) In the quantum response-function formalism, the R and NR signals for an isolated oscillator exhibit no variation with τ_2, while the DQC signal, although identical to the NR signal at $\tau_2 = 0$, oscillates rapidly at the $0 \rightarrow 2$ transition frequency (here ~10 fs). A nearly identical behavior is exhibited in the classical simulation; the R signal is static in time, while the NR/DQC signal displays two separate frequency components. At $\tau_2 = 0$, the two components are identical, each equal to half of the NR/DQC spectrum plotted in frame (a); as τ_2 varies, the first component is static in time, while the second oscillates with a period of ~10 fs, as illustrated in the inset of frame (a). In analogy to the quantum case, we regard the static NR/DQC component as the NR spectrum and the oscillatory component as the DQC spectrum.

This separation into distinct Fourier components suggests that, just as in the quantum case, we can obtain cleaner signals by combining the R and NR spectra to obtain pure absorptive features without the unsightly "phase twist" exhibited in frames (a)–(d).[31] The resulting correlation surfaces are presented in frames (e) and (f) and, indeed, take the form of purely absorptive features. Negative signals in the classical spectrum closely resemble the ground state bleach of the quantum spectrum, while positive signals resemble an induced-absorption feature.

These correlation surfaces allow for a straightforward comparison of the frequency differences between quantum and classical signals. Overall, the classical spectrum appears ~23 cm^{-1} higher in frequency than the quantum spectrum and exhibits a slightly lower apparent anharmonicity (the frequency difference between positive and negative features). In fact, the observed anharmonicity of the classical signal is determined almost entirely by the frequency resolution afforded by the simulated scan time of T_{scan} = 3 ps. In a higher-resolution simulation with T_{scan} = 20 ps [see the insets of frames (e) and (f)], the apparent anharmonicity is reduced to less than 3 cm^{-1}. This is in stark contrast to the 16 cm^{-1} anharmonicity of the quantum spectrum, which for $T_{scan} \geq 3$ ps is essentially independent of the scan time. Note that the similarity of quantum and classical spectra at low resolution reflects a similarity of the time-domain responses at short times, as observed in Refs. 20, 21, and 32.

These observations are suggestive of a weaker effective anharmonicity for the classical oscillator relative to its quantum counterpart. Physically, this observation can be understood as a zero-point energy effect since the uncertainty-limited width of the quantum ground state wave function ensures that the particle samples anharmonic regions of the potential even in the absence of thermal excitation. The classical oscillator, in contrast, is initially localized exactly at the minimum-energy—and thus the most harmonic—point in the Morse potential.

Finally, note that the observed identity of the NR and DQC signals at $\tau_2 = 0$ is extremely useful computationally. Formally, of course, the NR spectrum in a third-order signal should be isolated from the full signal via a Fourier filter in τ_2, as performed in Fig. 1. Considerable computational effort is avoided, however, if the NR spectrum is defined as half the NR/DQC signal at $\tau_2 = 0$; in what follows, we adopt this definition. For nonperturbative simulations, this convention has the considerable advantage that it is physically meaningful even in the presence of higher-order nonlinearities (fifth, seventh, etc.) which, due to the possibility of multiple interactions with

a single pulse, are expected to produce additional frequency components in τ_2. Indeed, as explored in Sec. II C, such signals become dominant in the classical simulation at even rather modest laser intensities.

C. Power dependence

It is informative to now investigate the dependence of the classical 2D signal on laser intensity. Frames (a) and (b) of Fig. 2 present the 2D correlation spectra of the Morse oscillator at $\tau_2 = 0$ for pulse powers of 0.1 nJ and 10 nJ, respectively, with a simulated scan time of T_{scan} = 20 ps. These classical signals may be directly compared with the quantum signal in the inset of frame (f) of Fig. 1; for these parameters, the quantum signal is dominated by the third-order response and so is essentially independent of fluence.[33] For the classical signals, we find qualitatively similar features but a continuous shift toward lower frequencies and larger apparent anharmonicities with increasing fluence. At 0.1 nJ, the bleaching signal appears above the diagonal at ω_3 = 1649.9 cm^{-1}, and the separation between bleach and induced-absorption figures is still resolution-limited with an apparent anharmonicity less than 2 cm^{-1}. At 10 nJ pulse energy, the bleach signal shifts below the diagonal to ω_3 = 1646.9 cm^{-1}, and the bleach and induced-absorption features are well resolved with an apparent anharmonicity of 2.6 cm^{-1}. In addition, in the 10 nJ spectrum, a weak positive feature is faintly visible above the diagonal, suggesting the presence of higher-order (fifth, seventh, etc.) signals. For higher pulse energies (not shown), this trend continues, with continuously decreasing signal frequencies and increasingly well-resolved bleach and induced-absorption features.

Further insight is offered by the τ_2-dependence of the signal, plotted in frame (c); blue corresponds to a pulse energy of 0.1 nJ, and green corresponds to 10 nJ. As in Fig. 1, the plotted signal is the normalized depth of the rephasing bleach, sampled at a fixed frequency corresponding to the maximum depth at $\tau_2 = 0$. As in Fig. 1, the rephasing signal is essentially static in time at 0.1 nJ; at a higher power, however, oscillations appear at approximate multiples of the laser frequency ω_L = 1650 cm^{-1}. In a quantum framework, these oscillations would be clear indicators of higher-order nonlinear processes involving multiple interactions with at least one of the three perturbing pulses; however, quantum theory predicts that such signals should appear only at much higher pulse energies. We will return to this observation in an analytic model where we find that high-order nonlinearities indeed provide a simple explanation for these features.

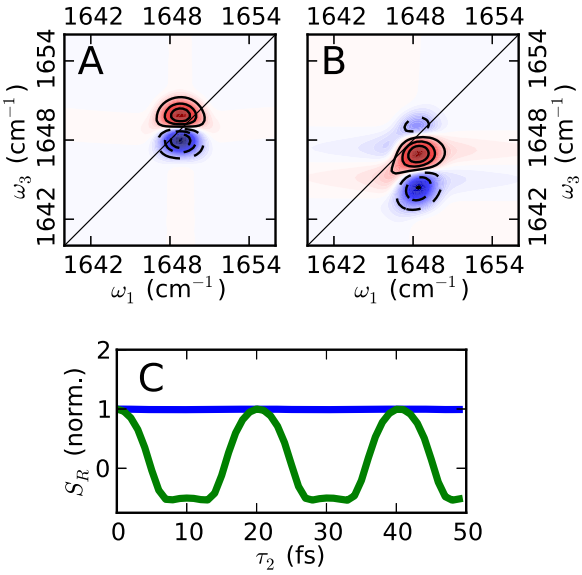

FIG. 2. High-resolution 2D spectra for a classical Morse oscillator with T_{scan} = 20 ps and pulse energies of 0.1 nJ [frame (a)] and 10 nJ [frame (b)]. Frame (c) plots the depth of the rephasing bleaches as a function of τ_2; the blue line corresponds to 0.1 nJ pulse energy, and the green line corresponds to 10 nJ.

D. Cross peaks and classical beats

One of the signature features of 2D spectroscopy is its ability to detect correlation between energy eigenstates via the formation of off-diagonal cross-peaks. In classical spectroscopy, there are no quantum eigenstates, but correlations still exist between interacting vibrational modes. To explore the formation of cross-peaks in classical spectroscopy, the 2D simulation results for a pair of coupled Morse oscillators with antiparallel [frames (a), (c), and (e)] or perpendicular [frames

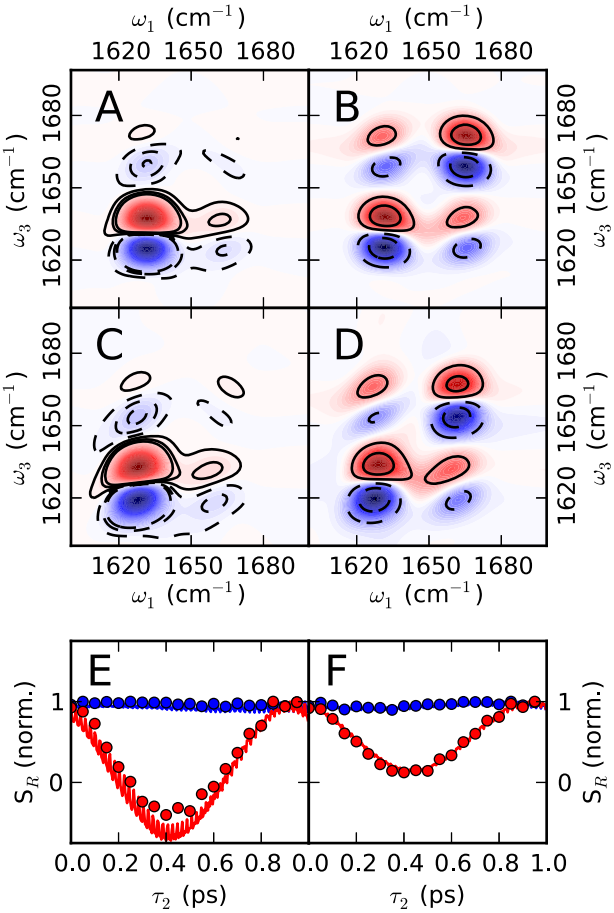

FIG. 3. Classical 2D correlation spectra for a pair of coupled Morse oscillators, together with time traces in τ_2 of the rephasing bleach. Frames (a), (c), and (e) are for a dimer with antiparallel dipole moments; frames (b), (d), and (f) are for a dimer with perpendicular dipole moments. Frames (a) and (b) are at T = 0 K; frames (c) and (d) are at T = 300 K. In frames (e) and (f), the lines represent traces at T = 0 K, while the filled circles represent traces at T = 300 K.

(b), (d), and (f)] dipoles are presented in Fig. 3. In both geometries, the isolated frequencies of the two oscillators are set to 1657.5 cm^{-1} and 1642.5 cm^{-1}, and the bilinear interaction potential is scaled so as to correspond in the quantum case to a 15 cm^{-1} coupling constant. For the simulation with perpendicular dipoles, orientational averaging is accomplished using the standard procedure[34] for a third-order spectroscopy.[35] For the antiparallel geometry, such parameters might, for example, model a pair of Amide I cross-strand nearest-neighbors in an antiparallel β-sheet. Frames (a) and (b) of Fig. 3 show the 2D correlation surfaces for the two geometries with $\tau_2 = 0$ and a pulse energy of 2 nJ. As in the quantum case (not shown), coupling between the oscillators shifts the frequencies of the two diagonal features, suppresses the amplitude of the higher-frequency mode, and produces cross-peaks in the off-diagonal regions. Note that for the antiparallel geometry, black contours are plotted only from −0.1 to +0.1 times the amplitude of the enhanced low-frequency peak to emphasize the low-amplitude cross-peak features.

Repeating the simulation as a function of τ_2 reveals that classical spectroscopy matches its quantum analog in the beating patterns observed in both diagonal and cross-peak features. Frames (e) and (f) of Fig. 3 present the normalized amplitude traces for the diagonal (blue lines) and cross-peak (red lines) features of the rephasing bleach. Just as in the quantum case, beating signals are obtained in the rephasing cross-peak, with a frequency corresponding to the splitting between diagonal features. Additional high-frequency small-amplitude oscillations can be observed in both diagonal and off-diagonal features, reflecting weak contributions from higher-order nonlinearities; the amplitude of these signals increases with increasing pulse energy.

An important conceptual question for vibrational spectroscopy is whether coherent signals persist at ambient temperature. Although our simulations so far correspond to a low-temperature limit (since the oscillator is initially at rest), it is expected *a priori* that increased temperatures should have little effect on the spectrum for the systems studied here. Indeed, even at room temperature, an $\omega_o = 1650$ cm^{-1} Morse oscillator is confined to a narrow region of the potential so that the frequencies sampled by the thermal ensemble are comparable to those in the $T = 0$ K limit. To check this prediction, we repeated the simulation of the coupled dimer for an ensemble of randomly sampled initial configurations for the coupled system from the $T = 300$ K Boltzmann distribution (see Appendix A for further computational details). The resulting averaged surfaces are presented in frames (c) and (d) of Fig. 3, while the τ_2-dependence of the signal is illustrated in frames (e) and (f) by closed circles. Aside from a slight shift toward lower frequencies, reflecting a thermal shift of the population away from the harmonic minimum, and the addition of some sampling noise, the signals are seen to be essentially unchanged from the $T = 0$ K result.

III. A NONPERTURBATIVE MODEL

These results demonstrate clearly that classical theory can provide a conceptually simple description of 2D vibrational spectroscopy for weakly anharmonic systems. This finding may seem at odds with the well-known instability of classical nonlinear response functions,[36–39] documented generally by Kryvohuz and Cao for integrable anharmonic systems.[21] To reconcile these apparently conflicting results, we consider the physical origins and significance of the classical divergence of nonlinear response functions for a simple nonperturbative analytical model.

A. A single-pulse measurement

As a preliminary example, consider the dynamics of a single anharmonic oscillator that is initially at rest and perturbed by an electric field of the form

$$E(t) = \frac{E_o}{\sqrt{2\pi\tau_L^2}} e^{-\frac{(t-t_o)^2}{2\tau_L^2}} \cos\omega_L(t-t_o). \tag{4}$$

The interaction Hamiltonian is described by the linear form

$$V(t) = -x\mu_o E(t), \tag{5}$$

where $x\mu_o$ is the oscillator dipole moment.

For an harmonic oscillator, the interaction of the system with the perturbing field can be evaluated analytically. In the short-pulse limit, the motion of the oscillator at times $t > 0$ is simply

$$x(t) = \frac{\mu_o E_o}{2\omega_o} \sin\omega_o t, \tag{6}$$

where ω_o is the oscillator frequency. For an anharmonic oscillator, the dynamics are more complicated and cannot be solved exactly. As a simple approximation, however, assume a weakly anharmonic oscillator, with the sole deviation from harmonicity appearing in the dependence of the oscillation frequency on the amplitude of the motion. In place of $\sin\omega_o t$, we thus write $\sin\omega t$, where $\omega = \omega(a)$ is a function of the amplitude a of the motion. For the Morse oscillator, for example, we have to first order in the anharmonicity[40]

$$\omega(a) \approx \omega_o\left(1 - \frac{\omega_o^2 a^2}{4D}\right), \tag{7}$$

where D is the dissociation energy. Physically, this decrease in frequency results from the slowed acceleration of the oscillator in regions of the potential with lower curvature.

As the intensity of the perturbing field approaches zero, this oscillation frequency ω converges to the limiting value ω_o, representing small displacements around equilibrium. For sufficiently weak fields, the dynamics will thus be well described by the linear approximation

$$x(t) \approx \alpha_o \sin\omega_o t, \tag{8}$$

where

$$\alpha_o = \frac{\mu_o E_o}{2\omega_o} \tag{9}$$

The range of field strengths for which this approximation accurately describes the dynamics is the linear response regime.

Suppose now we wish to determine, for some finite field strength E_o, the nonlinear component of the response. By

definition, this is the difference between the actual oscillator dynamics and the linearized approximation of Eq. (8), i.e.,

$$x_{NL}(t) = \alpha_o (\sin \omega t - \sin \omega_o t) = 2\alpha_o \sin\left(\frac{\omega_o^3 \alpha_o^2}{8D} t\right) \cos\left(\frac{\omega + \omega_o}{2} t\right). \quad (10)$$

For any finite field strength E_o, the nonlinear component of the response is thus a stable bounded function of the time t. In the Fourier domain, this signal contains two peaks, corresponding to a loss in signal (relative to the linear response) at the fundamental frequency ω_o and an increase in signal at the anharmonically induced frequency ω. This nonlinear component thus looks very much like the pump-probe response of a quantum system, which shows a bleach at the frequency of the linear $0 \rightarrow 1$ transition and an induced absorption at the frequency of the $1 \rightarrow 2$ transition. The key difference classically is that, as we saw in our numerical simulations, the frequency ω of the induced absorption is a function of the excitation intensity since it depends on how far into the anharmonic region of the potential the oscillator is driven.

In an effort to isolate a second-order signal, consider now the limit that $E_o \rightarrow 0$ and hence $\omega \rightarrow \omega_o$. The last factor in Eq. (10) converges to a cosine signal at the fundamental frequency ω_o. The sine term, however, represents a low-frequency modulation whose period increases without limit as E_o decreases. To the lowest order in α_o, we thus obtain the linearly divergent form

$$x_{NL}(t) \approx t \frac{\omega_o^3 \alpha_o^3}{4D} \cos(\omega_o t). \quad (11)$$

Although our total nonlinear signal is stable and bounded, it approaches a linearly divergent form when extrapolated to zero fluence. The only exception is for an harmonic system, where ω is independent of the field strength.

Although this result is overly simplistic in several respects, it neatly illustrates the type of divergence demonstrated much more generally by Kryvohuz and Cao.[21] Just as in our example, these divergences are not due to an underlying instability of classical mechanics; rather they are a result of the continuous range of dynamical frequencies that are classically allowed.[21] For a quantized system, the decreasing frequency gap $\omega - \omega_o$ of Eq. (10) would eventually converge to some minimum frequency difference between quantized energy levels; indeed, the divergence may be eliminated completely by introducing *ad hoc* discreteness into the dynamics.[41] In a classical system, no such minimum frequency difference exists, and hence classical response functions generically diverge in time.

B. 2D signals

It is straightforward to extend this model to describe the three-pulse experiments relevant to 2D spectroscopy. As detailed in Appendix B, we obtain a 2D signal:

$$S_{2D} = \frac{\mu_o^2 E_o}{2\omega_o} [\sin \omega_{123}\tau_3 + \sin \omega_1 \tau_3 - \sin \omega_{23}\tau_3 - \sin \omega_{13}\tau_3], \quad (12)$$

where $\omega_1, \ldots, \omega_{123}$ are the anharmonic oscillation frequencies of the oscillator after perturbation by all three pulses (ω_{123}), a pair of pulses (ω_{13} and ω_{23}), or a single pulse (ω_1).

There are two key observations to make regarding this result. First, each multi-pulse oscillation frequency depends sensitively on the time delay between the various pulses in the experiment. For example, an oscillator excited by pulses 1 and 2 (separated by time delay τ_1) oscillates with a frequency

$$\omega_{12} \approx \omega_o \left(1 - \frac{\mu_o^2 E_o^2}{4D} \cos^2 \frac{\omega_1}{2} \tau_1\right). \quad (13)$$

This frequency modulation reflects the fact that an excited oscillator may be driven further from or back toward equilibrium, depending on the relative phase of the oscillator and the driving field. When excitation is in phase with the oscillator's motion (i.e., τ_1 is an integer multiple of $\frac{2\pi}{\omega_1}$), the oscillation frequency is maximally anharmonic, reflecting the two pulses working together to drive the oscillator away from equilibrium. Conversely, when the two pulses are exactly out of phase, the oscillation frequency drops to the limiting value ω_o, reflecting the driving of the oscillator back to its equilibrium position. It is through this frequency modulation of the signal in τ_3 that information regarding interactions with the first two pulses is encoded.

Second, the response is highly nonlinear in the amplitude E_o of the perturbing field. In fact, since the deviation of each frequency ω_n from the limiting value ω_o is quadratic in E_o, the lowest-order contribution to the expansion is of third order [see Eq. (B12)]:

$$S_{2D} \approx -\tau_3 \frac{\mu_o^4 E_o^3}{16\omega_o D} \cos \omega_o \tau_1 \cos \omega_o \tau_3. \quad (14)$$

For short times, the signal thus increases linearly in τ_3, much like the divergent third-order response function.[21] At longer times, however, higher-order nonlinearities eventually force it back into the periodic variation indicated by Eq. (12). Physically, the time scale of this linear divergence carries considerable significance since it determines the effective splitting along the ω_3 axis between bleaching and induced-absorption features.[42]

In terms of this simple model, we can easily rationalize several features of the above numerical simulations. For low pulse energies, the linear "divergence" of Eq. (14) occurs over a time scale that is long relative to our detection window. The resulting 2D spectrum exhibits closely-spaced fundamental and overtone features, closely resembling the quantum result but with a very weak anharmonicity. At higher pulse energies, the effective anharmonicity increases and higher-order nonlinearities begin to appear, as observed in Fig. 2.

A perhaps more interesting prediction of this model is that nonlinearities higher than third-order should grow in not only with increasing pulse energy but also with longer detection time scales. At short times, as seen above, the third-order signal dominates; at longer times, fifth- and higher-order processes gradually become more significant. In spectroscopic terms, this suggests the somewhat counter-intuitive notion that a high-resolution low-fluence 2D spectrum should—in the appearance of higher-order features—mimic a low-resolution high-fluence spectrum.

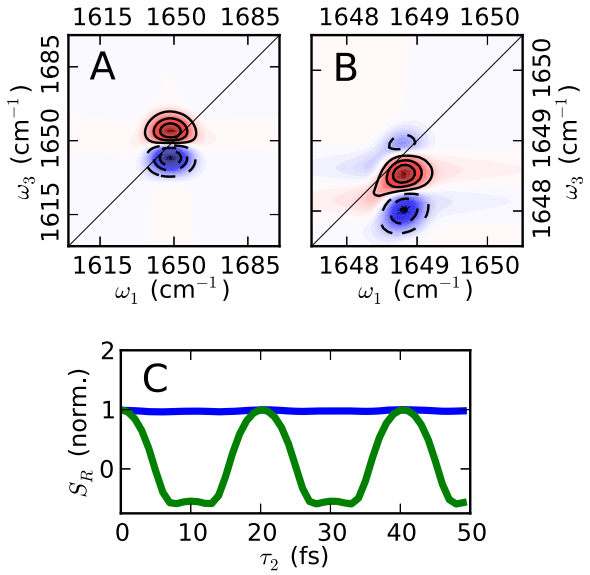

FIG. 4. Classical 2D spectra for a single Morse oscillator at a pulse energy of 2 nJ and scan times of 3 ps [frame (a)] or 50 ps [frame (b)]; note the different frequency scales for the two plots, reflecting the higher-resolution afforded by the 50 ps scan time. Frame (c) plots the depth of the rephasing bleach for each spectrum as a function of τ_2; blue corresponds to T_{scan} = 3 ps, and green corresponds to T_{scan} = 50 ps.

This suggestion is easily tested numerically. Figure 4 compares the correlation surfaces and rephasing-bleach time traces [frame (c)] for a single Morse oscillator with a pulse energy of 2 nJ and simulated scan times of T_{scan} = 3 ps [frame (a), as in Fig. 1] and T_{scan} = 50 ps [frame (b)]. As predicted by the analytical model, the high-resolution spectrum shows the feature characteristic of higher-order nonlinear processes: the bleaching signal is shifted below the diagonal (plotted as a thin black line for reference), and weak induced-absorption signals are beginning to appear above the diagonal, just as in the 10 nJ spectrum of Fig. 2. (Note the difference in frequency scales on the two plots.) These features are even more apparent in the rephasing-bleach τ_2 traces presented in the lower panel of Fig. 4. At low resolution, the signal is static in time, indicating the dominance of third-order processes. At high resolution, strong beating signals appear, identical in form to those obtained at high pulse energy in Fig. 2.

Finally, although an explicit description of the coupled-oscillator case is more complicated, it is not difficult to see physically how coupling produces spectroscopic features such as cross peaks and coherent beating in classical 2D spectra. For weak anharmonicity, the coupled system may again be treated as effectively harmonic, but with a set of normal mode frequencies and coefficients that depend on the total excitation energy of the system. As a result, repeated excitation of each normal mode modifies not only its own oscillation frequency (resulting in the diagonal peaks already discussed) but also the frequencies of other coupled modes, producing cross peaks in the 2D spectrum. Coherent beating signals—one might say "classical beats"—in τ_2 likewise arise naturally as a result of normal mode oscillations coming in and out of phase with one another on a time scale inversely proportional to their frequency difference.

IV. DISCUSSION

A. Classical spectroscopy

The key result of this study is that classical mechanics admits of a well-defined conceptual description of nonlinear vibrational spectroscopy, even when nonlinear response theory fails. This finding is consistent with, for example, the observation of van Kampen nearly a half-century ago that, at the molecular scale, even macroscopically weak perturbations can induce highly nonlinear dynamics.[43] In short, at the microscopic scale, there is no such thing as a "weakly nonlinear" perturbation to a non-dissipative classical system; on some time scale, all perturbations are highly nonlinear. Therefore, as van Kampen argued, reliance on the nonlinear response framework can obscure interesting physics.

At the same time, our comparison of quantum and classical signals highlights the critical role that quantization plays in stabilizing nonlinear response, a distinction that is perhaps unclear in van Kampen's discussion. Whereas the continuous range of frequencies available to a classical anharmonic oscillator defies the separation of its response into an orderly power series, the quantized oscillator possesses a natural energy scale (the eigenstate splitting) below which perturbations can rigorously be considered weak. In spectroscopic terms, this distinction between classical and quantized responses is neatly illustrated by the continuous variation of signal frequencies and anharmonicity observed in the classical 2D surfaces with changing pulse power. Indeed, for closed systems, this continuous tuning might well be regarded as a defining feature of classicality. Conversely, the appearance of clearly resolved transition frequencies that do not shift with excitation power seems (for closed systems) to be a distinctly quantum-mechanical feature.

For open systems, the situation is complicated by dissipation and dephasing induced by the environment. Although such processes are beyond the scope of this work, it should be noted that the generic divergence demonstrated by Kryvohuz and Cao[21] applies only to closed integrable systems. The nonlinear response of chaotic systems is much less well understood.[44] Moreover, it is entirely possible for an *open* classical system to possess stable response functions.[39] Indeed, if a system returns to equilibrium on a characteristic time scale τ_{thermal}, one may expect its response to perturbation—and hence its response functions—to decay on a similar scale. This observation helps to explain why classical molecular dynamics (MD)-based methods for evaluating nonlinear response tensors have proven successful for some systems, notably the 2D IR calculations of Jeon and Cho[45,46] and the 2D Raman simulations of various groups.[29,47–50] Even if thermalization is not explicitly included in such simulations, the high dimensionality afforded by an explicit solvent provides an effective thermal environment for the oscillator of interest. Moreover, from a practical standpoint, the long-time stability of such simulations may be of supplementary interest since the short-time response may already provide a useful probe of system dynamics.

Finally, it should be noted that strong system-bath interactions can even bring quantum and classical predictions for nonlinear response into agreement with each other.[39] Indeed,

if thermalization occurs on a time scale that is short relative to the frequency gap between quantized energy levels, one may expect classical and quantum predictions to be similar since dissipation effectively coarse-grains over the quantized energy levels. This convergence is illustrated nicely in Ref. 51, where quantum and classical computations for the third-order response tensor for a dissipative system are found to largely agree for strong (but not for weak) system-bath interactions. (Note, however, that in that work only the absolute value of the 2D signal is calculated so that in the presence of strong dephasing the distinct signs of the fundamental and overtone transitions are not resolved.) Qualitatively, then, classical theory should be expected to provide an accurate description of nonlinear spectroscopy for systems where environmental damping is large relative to vibrational anharmonicity. By the same token, one may speculate—although our closed-system results provide no direct evidence—that well-separated, fluence-independent fundamental and overtone frequencies may serve as an indicator for quantum behavior in open systems as well as closed systems. A definitive test of this suggestion, however, requires a more general study of the nonlinear spectroscopic properties of open systems.

B. Coherence in ultrafast spectroscopy

Returning now to the physical interpretation of 2D signals, our results demonstrate that the coherent dynamics often observed in 2D vibrational spectroscopies may be qualitatively understood as an essentially classical phenomenon. While quantization alters the effective anharmonicity of the dynamics, it evidently plays little role in producing the "quantum beats" characteristic of 2D signals in underdamped systems. This finding may be taken as a generalization to the fully classical case of previous results using semiclassical methods.[52,53] Thus, in developing a cohesive physical understanding of 2D vibrational spectroscopies, simple nonperturbative classical models may provide considerable conceptual clarity, if not quantitative accuracy. Rather than relying on population and coherence terms in a density matrix, such models offer a description of nonlinear spectroscopies in the considerably more concrete terms of mechanical oscillations entering and leaving resonance with one another.

To extend these results to electronic spectroscopy would require an assumed electronic potential energy surface. In contrast to the vibrational case, however, the physical relevance of a classical electronic potential is unclear.[54] In a fully classical framework, there thus appears to be no direct and physically unambiguous extension of our results to the electronic domain. However, Loring and co-workers have demonstrated that semiclassical quantization provides an accurate description of both vibrational and electronic 2D surfaces.[52,53,55,56] Indeed, at least to this point, there appears to be little evidence that more exotic quantum features[57] such as wave-particle duality or entanglement (as distinct from classical correlation) play a significant role in any classical-light 2D experiment. In short, semiclassical quantization appears to be the key quantum-mechanical ingredient for 2D spectroscopy.

V. CONCLUSIONS

In conclusion, we have demonstrated through nonperturbative numerical simulations that the key qualitative features of 2D vibrational spectroscopy are well described by classical dynamics, even for systems for which the nonlinear response expansion fails. In addition, we describe a simple nonperturbative model which analytically captures the essential features of classical 2D signals for weakly anharmonic systems and offers useful insight into the classical divergence of nonlinear response functions. This suggests that nonperturbative classical models can offer a useful resource in developing a cohesive physical description of nonlinear spectroscopic experiments. A particularly interesting feature of these classical simulations is that they capture the coherent beating patterns sometimes observed in 2D vibrational spectroscopy. This observation makes clear that such features cannot be regarded as hallmarks of quantum mechanics but may be equally well understood classically. Instead, our findings indicate that the essential distinction between quantum and classical mechanics is the same in both linear and nonlinear spectroscopies: the semiclassical quantization of transition frequencies.

ACKNOWLEDGMENTS

M.R. thanks the Natural Sciences and Engineering Research Council of Canada (NSERC) for a Banting Postdoctoral Fellowship. Partial support for this work was provided by the AFOSR under Contract No. FA9550-13-1-0005. Computations were performed on the GPC supercomputer at the SciNet HPC Consortium. SciNet is funded by the Canada Foundation for Innovation under the auspices of Compute Canada; the Government of Ontario; Ontario Research Fund-Research Excellence; and the University of Toronto.

APPENDIX A: COMPUTATIONAL DETAILS

1. Model parameters

For single-oscillator simulations, we study an oscillator subject to the Morse potential

$$v(x) = D\left(1 - e^{-\kappa x}\right)^2, \tag{A1}$$

where

$$\kappa = \sqrt{\frac{M\omega_o^2}{2D}}, \tag{A2}$$

with M being the oscillator mass, ω_o being the harmonic frequency of the potential, and D being the anharmonicity. For multi-oscillator simulations, we consider two such oscillators with coordinates x_1 and x_2 coupled by a bilinear interaction term Jx_1x_2.

Model parameters are chosen as typical for the Amide I vibrational group (peptide backbone C=O stretch), which has been extensively studied via 2D IR spectroscopy.[58] The oscillator mass M is equal to the reduced mass of the C=O oscillator, i.e., $M \approx 6.86$ amu. Harmonic frequencies are in the range of 1600–1700 cm^{-1}, as reported in the text. The anharmonicity D is set to $50.5\hbar\omega_o$, in order to reproduce, in the quantized oscillator, the experimentally measured anharmonicity of 16 cm^{-1} for Amide I vibrations. For comparison

with quantum simulations, the value of J is reported in units of cm^{-1}

$$J(\text{cm}^{-1}) = \frac{\hbar}{2M\omega_o}J, \tag{A3}$$

representing the coupling matrix element $\langle 10|Jx_1x_2|01\rangle$ between two harmonic oscillators in the single-excitation manifold. The transition dipole moment strength is set to the experimentally measured value[59] of ~0.12 D^2. In the harmonic dipole approximation,

$$\langle 1|q_i|0\rangle = \sqrt{\frac{\hbar}{2\omega_{10}}}, \tag{A4}$$

this gives an estimate of $|\boldsymbol{\mu}_i| \approx 3.4\,\text{D}/(\text{Å amu}^{\frac{1}{2}})$ (i.e., ≈8.9 D/Å in unweighted coordinates).

The pulse width τ_L of the incident laser field is set to 20 fs. The amplitude of the perturbing field is determined by the pulse energy employed in each simulation. For converting between field amplitude and pulse power, we assume a 25 μm-diameter beam size so that a 2 nJ pulse energy corresponds to a maximum field amplitude of ~3 MV/cm. All simulations are carried out in the ZZZZ polarization sequence, i.e., all excitation polarizations are identical to the final detection polarization. Note that these parameters represent ideal experimental conditions (ultrafast pulses, Gaussian profiles, etc.) and that the response is evaluated for perfect alignment between the perturbed oscillator and the laser field. For a given pulse power, our calculated response is thus expected to be somewhat larger than would be observed in a typical experiment.

2. MD simulations

Classical oscillator simulations were carried out by MD integration using the velocity-Verlet algorithm[60] under the explicit force due to the electric laser field. For simulations at finite temperature, the system was initialized at rest at the potential energy minimum and then thermalized to the Boltzmann ensemble by propagation under Langevin dynamics using the modified Verlet-type integrator of Ref. 60. Langevin thermalization employed a friction coefficient of $\gamma = 0.1$ amu/fs and an equilibration period of 7 ps, i.e., 10 times the single-particle relaxation time $\tau_{\text{rel}} = M/\gamma \approx 70$ fs. The equilibrated system was then propagated under deterministic velocity-Verlet dynamics during the interaction with the perturbing fields. For $T = 300$ K simulations, ensembles of 320 000 random samples were employed for the $\tau_2 = 0$ fs spectra plotted in Fig. 3. For $\tau_2 \neq 0$, the simulation ensembles consisted of 80 000 realizations for the antiparallel dimer and 40 000 realizations for the perpendicular dimer. All simulations were carried out on the GPC supercomputer at the SciNet HPC Consortium.[61]

3. Signal processing

The sample polarization

$$\boldsymbol{P}(t) = \langle \boldsymbol{\mu}(t)\rangle \tag{A5}$$

was calculated explicitly from classical MD simulations. The averaging brackets here refer to finite-temperature simulations noted above. This polarization vector is then converted to a spectroscopic signal by explicitly heterodyning against the amplitude of the final pulse, i.e., the time-domain signal is calculated as the Fourier transform of the frequency-domain product between the polarization vector $\boldsymbol{P}$ and the time-derivative of the electric field vector $\boldsymbol{E}$ due to the last pulse. (The time derivative here accounts for the $\frac{\pi}{2}$ phase shift associated with emission of the electromagnetic field from the sample.[62])

Note that, although phase-matching is not explicitly considered in these simulations, it is automatically enforced by the fact that the signal amplitude is monitored only in the experimentally relevant frequency range near 1650 cm^{-1}. Since all generated signals must approximately satisfy the sum restriction $\omega_s = \sum_i \omega_i$ (where the interaction frequencies ω_i are plus or minus the laser frequency $\pm\omega_L$), the corresponding propagation wavevectors are likewise expected to satisfy the wavevector-matching condition $\boldsymbol{k}_s = \sum_i \boldsymbol{k}_i$, so long as each interaction wavevector $\boldsymbol{k}_i$ is either parallel or antiparallel to the same propagation axis. The simulation results thus match the signal generated experimentally in an all-collinear geometry where phase-matching for the propagated signal is automatically enforced by frequency conservation.

Finally, the spectroscopic signal is converted to a 2D spectrum via the double Fourier transform

$$S(\omega_1,\tau_2,\omega_3) = \Re \int d\tau_1 \int d\tau_3 e^{i\omega_1\tau_1} e^{i\omega_3\tau_3} \times S_{123}(\tau_3;\tau_2,\tau_1)W(\tau_1)W(\tau_3) \tag{A6}$$

where $W(\tau)$ is a windowing function that avoids numerical instability in the discrete Fourier transform by ensuring that the signal converges smoothly to zero outside of the simulation window.

APPENDIX B: ANALYTICAL MODEL

As described in the text, we consider the dynamics of an anharmonic oscillator perturbed by a series of three laser pulses. To make the calculation tractable, a series of approximations applicable to weakly anharmonic systems and weak ultrafast pulses are adopted.

First, the oscillator motion is assumed to be a simple sinusoidal variation in time, with a frequency that depends on the amplitude of the motion:

$$x(t) = a\ \sin\left(\omega(a)t + \phi\right), \tag{B1}$$

that is, higher-frequency Fourier components[40] that in general should appear at integer multiples of $\omega(a)$ are neglected. (This approximation will necessarily prevent our model from capturing the DQC signal which involves oscillations at ~$2\omega_o$.) For a Morse oscillator, the frequency of motion can be expanded to the first order in the anharmonicity of the potential (as measured by the inverse dissociation energy D^{-1}) as[40]

$$\omega(a) \approx \omega_o\left(1 - \frac{\omega_o^2 a^2}{4D}\right), \tag{B2}$$

a form assumed for all analytical calculations.

Second, we assume that the dynamics of the oscillator's interaction with the pulse may (for very short pulses) be treated approximately harmonically. For an harmonic oscillator initially in the state described by Eq. (B1), interaction with a

Gaussian pulse of form 4 induces in the limit $\tau_L \to 0$ the perturbed motion

$$x'(t) = a\ \sin(\omega_o t + \phi) + \alpha_o\ \sin\ \omega_o(t - t_o) \tag{B3}$$

for times $t > t_o$, with

$$\alpha_o = \frac{\mu_o E_o}{2\omega_o}. \tag{B4}$$

For the anharmonic oscillator, the same form is assumed for the post-interaction motion, but the oscillation frequency in the two terms is allowed to differ:

$$x'(t) = a\ \sin(\omega_a t + \phi) + \alpha\ \sin\ \omega_{a'}(t - t_o) \tag{B5}$$

where

$$\alpha = \frac{\mu_o E_o}{\omega_a + \omega_{a'}} \approx \alpha_o \left(1 - \frac{\delta\omega_a + \delta\omega_{a'}}{2\omega_o}\right) \tag{B6}$$

and a' is the amplitude of the post-interaction motion (taking $t = t_o$)

$$a' = \left[a^2 + \alpha^2 + 2a\,\alpha\ \cos(\phi + \omega_a t_o)\right]^{\frac{1}{2}}. \tag{B7}$$

Within these approximations, we can easily evaluate the oscillator response in a multi-pulse experiment. We denote by x_k the position of the perturbed oscillator in an experiment involving only pulse $k = 1, 2$, and 3; similarly, x_{jk} is the position of an oscillator in an experiment involving both pulses $j < k$, and x_{123} is the position of the oscillator perturbed by all three pulses. Then

$$x_k = \alpha_o \left(1 - \frac{\delta\omega_1}{2\omega_o}\right) \sin\ \omega_1(t - t_o^{(k)}) \tag{B8a}$$

$$\begin{aligned} x_{jk} &= x_j + \alpha_o \left(1 - \frac{\delta\omega_1 + \delta\omega_{jk}}{2\omega_o}\right) \sin\ \omega_{jk}(t - t_o^k) \\ &= 2\alpha_o \cos\left(\frac{\omega_j}{2}\tau_{jk}\right) \sin\left(\omega_{jk}(t - t_o^{(k)}) + \frac{\omega_j}{2}\tau_{jk}\right) \end{aligned} \tag{B8b}$$

$$x_{123} = x_{12} + \alpha_o \left(1 - \frac{\delta\omega_{12} + \delta\omega_{123}}{2\omega_o}\right) \sin\ \omega_{123}(t - t_o^{(3)}), \tag{B8c}$$

where $\tau_{jk} = t_o^{(k)} - t_o^{(j)}$, and for the Morse oscillator,

$$\omega_1 \approx \omega_o \left(1 - \frac{\mu_o^2 E_o^2}{16D}\right) \tag{B9a}$$

$$\omega_{jk} \approx \omega_o \left(1 - \frac{\mu_o^2 E_o^2}{4D} \cos^2 \frac{\omega_o}{2}\tau_{jk}\right) \tag{B9b}$$

$$\begin{aligned} \omega_{123} \approx \omega_o \Bigg(1 - \frac{\mu_o^2 E_o^2}{4D} \Bigg[\frac{1}{4} + \cos^2 \frac{\omega_o}{2}\tau_1 \\ + \cos \frac{\omega_o}{2}\tau_1 \cos\left(\frac{\omega_o}{2}\tau_1 + \omega_o\tau_2\right)\Bigg]\Bigg). \end{aligned} \tag{B9c}$$

Note that in all cases only terms to linear order in the anharmonicity D^{-1} have been retained.

As discussed in the main text, the component of the response relevant to 2D spectroscopy is

$$\begin{aligned} x_{2D} &= x_{123} - x_{12} - (x_{23} - x_2) - (x_{13} - x_1) + x_3 \\ &= \alpha\left[\sin\ \omega_{123}\tau_3 + \sin\ \omega_1\tau_3 - \sin\ \omega_{23}\tau_3 - \sin\ \omega_{13}\tau_3\right]. \end{aligned} \tag{B10}$$

Although written explicitly as only a function of τ_3, the signal implicitly depends on the time delays τ_1 and τ_2 through the various frequency terms. For an harmonic system (with all frequencies equal to ω_o), the response vanishes, as expected. In the linearized approximation,

$$\sin\ x + \varepsilon = \sin\ x + \varepsilon\ \cos\ x, \tag{B11}$$

we obtain to third-order in the perturbing field E_o

$$\begin{aligned} x_{2D} &\approx \tau_3\alpha\left[\omega_{123} - \omega_{23} - \omega_{13} + \omega_1\right] \cos\ \omega_o\tau_3 \\ &= -\tau_3 \frac{\mu_o^3 E_o^3}{16\omega_o D} \cos\ \omega_o\tau_1 \cos\ \omega_o\tau_3. \end{aligned} \tag{B12}$$

[1] W. Zhuang, T. Hayashi, and S. Mukamel, Angew. Chem., Int. Ed. **48**, 3750 (2009).
[2] F. Milota, J. Sperling, A. Nemeth, T. Mančal, and H. F. Kauffmann, Acc. Chem. Res. **42**, 1364 (2009).
[3] M. Cho, T. Brixner, I. Stiopkin, H. Vaswani, and G. R. Fleming, J. Chin. Chem. Soc. **53**, 15 (2006).
[4] A. L. Le Sueur, R. E. Horness, and M. C. Thielges, Analyst **140**, 4336 (2015).
[5] T. Elsaesser, Acc. Chem. Res. **42**, 1220 (2009).
[6] G. S. Engel, T. R. Calhoun, E. L. Read, T.-K. Ahn, T. Mančal, Y.-C. Cheng, R. E. Blankenship, and G. R. Fleming, Nature **446**, 782 (2007).
[7] G. Panitchayangkoon, D. Hayes, K. A. Fransted, J. R. Caram, E. Harel, J. Wen, R. E. Blankenship, and G. S. Engel, Proc. Natl. Acad. Sci. U. S. A. **107**, 12766 (2010).
[8] E. Romero, R. Augulis, V. I. Novoderezhkin, M. Ferretti, J. Thieme, D. Zigmantas, and R. van Grondelle, Nat. Phys. **10**, 676 (2014).
[9] E. Collini, C. Y. Wong, K. E. Wilk, P. M. G. Curmi, P. Brumer, and G. D. Scholes, Nature **463**, 644 (2010).
[10] G. D. Scholes, G. R. Fleming, A. Olaya-Castro, and R. van Grondelle, Nat. Chem. **3**, 763 (2011).
[11] N. Christensson, H. F. Kauffmann, T. Pullerits, and T. Mančal, J. Phys. Chem. B **116**, 7449 (2012).
[12] V. Tiwari, W. K. Peters, and D. M. Jonas, Proc. Natl. Acad. Sci. U. S. A. **110**, 1203 (2013).
[13] H.-G. Duan, V. I. Prokhorenko, R. J. Cogdell, K. Ashraf, A. L. Stevens, M. Thorwart, and R. J. D. Miller, Proc. Natl. Acad. Sci. U. S. A. **114**, 8493 (2017).
[14] X. Jiang and P. Brumer, J. Chem. Phys. **94**, 5833 (1991).
[15] P. Brumer and M. Shapiro, Proc. Natl. Acad. Sci. U. S. A. **109**, 19575 (2012); A. Dodin, T. V. Tscherbul, and P. Brumer, J. Chem. Phys. **145**, 244313 (2016).
[16] E. N. Zimanyi and R. J. Silbey, J. Chem. Phys. **133**, 144107 (2010).
[17] J. S. Briggs and A. Eisfeld, Phys. Rev. E **83**, 051911 (2011).
[18] W. H. Miller, J. Chem. Phys. **136**, 210901 (2012).
[19] S. Duque, P. Brumer, and L. A. Pachón, Phys. Rev. Lett. **115**, 110402 (2015).
[20] M. Kryvohuz and J. Cao, Phys. Rev. Lett. **95**, 180405 (2005).
[21] M. Kryvohuz and J. Cao, Phys. Rev. Lett. **96**, 030403 (2006).
[22] F. D. Fuller and J. P. Ogilvie, Annu. Rev. Phys. Chem. **66**, 667 (2015).
[23] R. Kubo, J. Phys. Soc. Jpn. **12**, 570 (1957).
[24] In principle, this numerical filtering approach is quite general and requires no prior knowledge of the system response. In practice, of course, the utility of the method will depend on the complexity of system studied and, in particular, on the computational effort required to propagate the system dynamics with a small enough time-step and a long enough time scale to accurately resolve all frequency components.
[25] Note that since T_{scan} sets the time scale over which the signal is nonzero, it may also be considered analogous to the dephasing or relaxation time of a condensed-phase (non-isolated) oscillator.
[26] For a disordered sample, geometric averaging should in principle be included to account for the distribution of molecular orientations with respect to the laser field, but in the case of a single oscillator this would result only in an average over effective pulse energies.
[27] C. Dellago and S. Mukamel, Phys. Rev. E **67**, 035205(R) (2003).
[28] C. Dellago and S. Mukamel, J. Chem. Phys. **119**, 9344 (2003).
[29] T. l. C. Jansen, J. G. Snijders, and K. Duppen, J. Chem. Phys. **113**, 307 (2000).
[30] P. Lynch, Mon. Weather Rev. **125**, 655 (1997).

[31]M. Khalil, N. Demirdöven, and A. Tokmakoff, Phys. Rev. Lett. **90**, 047401 (2003).
[32]W. G. Noid, G. S. Ezra, and R. F. Loring, J. Phys. Chem. B **108**, 6536 (2004).
[33]As a simple estimate, note that the quantum nth-order response is scaled by a prefactor $a_n \approx (2\pi)^{\frac{n}{2}} \left(\frac{\tau_p \mu_o E_o}{\hbar}\right)^n$, where τ_p is the pulse length, μ_o is the relevant transition dipole matrix element, E_o is the maximum amplitude of the field in the sample, and the factor $\sqrt{2\pi}$ comes from the assumption of a Gaussian pulse envelope. For our parameters and a pulse energy of 10 nJ, $a_5/a_3 \approx 0.15$, confirming that the nonlinear signal is dominated by third-order response.
[34]C. R. Baiz, M. Reppert, and A. Tokmakoff, in *Ultrafast Infrared Vibrational Spectroscopy*, edited by M. D. Fayer (CRC Press, Boca Raton, 2013), pp. 361–404.
[35]To the extent that higher-order interactions are present in the signal, this will introduce some error in the peak intensities but is unlikely to affect the qualitative results. No such difficulty appears in the simulation with antiparallel dipoles since there is only a single molecular axis with which the laser field interacts.
[36]J. A. Leegwater and S. Mukamel, J. Chem. Phys. **102**, 2365 (1995).
[37]W. G. Noid, G. S. Ezra, and R. F. Loring, J. Chem. Phys. **120**, 1491 (2004).
[38]J. Wu and J. Cao, J. Chem. Phys. **115**, 5381 (2001).
[39]M. Kryvohuz and J. Cao, J. Chem. Phys. **130**, 234107 (2009).
[40]R. B. Shirts, J. Phys. Chem. **91**, 2258 (1987).
[41]M. Kryvohuz and J. Cao, J. Chem. Phys. **122**, 024109 (2005).
[42]Note that linear divergence in τ_3 may be associated approximately with a low-frequency sine function, corresponding in Fourier space to convolution with a positive-valued delta function at positive frequencies and a negative-valued delta function at negative frequencies.
[43]N. G. van Kampen, Phys. Norv. **5**, 279 (1971).
[44]S. V. Malinin and V. Y. Chernyak, Phys. Rev. E **77**, 056201 (2008).
[45]J. Jeon and M. Cho, New J. Phys. **12**, 065001 (2010).
[46]J. Jeon and M. Cho, J. Phys. Chem. B **118**, 8148 (2014).
[47]A. Ma and R. M. Stratt, Phys. Rev. Lett. **85**, 1004 (2000).
[48]S. Saito and I. Ohmine, J. Chem. Phys. **119**, 9073 (2003).
[49]T. Hasegawa and Y. Tanimura, J. Chem. Phys. **125**, 074512 (2006).
[50]H. Ito, J.-Y. Jo, and Y. Tanimura, Struct. Dyn. **2**, 054102 (2015).
[51]A. Sakurai and Y. Tanimura, J. Phys. Chem. A **115**, 4009 (2011).
[52]M. Gerace and R. F. Loring, J. Phys. Chem. B **117**, 15452 (2013).
[53]M. Alemi and R. F. Loring, J. Chem. Phys. **142**, 212417 (2015).
[54]The Coulomb potential, for example, is thermodynamically unstable for classical dynamics. Various weakly anharmonic forms could be assumed empirically, but in our simulations (not shown) these result in the formation of unphysical induced-absorption features in the electronic spectrum.
[55]M. Alemi and R. F. Loring, J. Phys. Chem. B **119**, 8950 (2015).
[56]R. F. Loring, J. Chem. Phys. **146**, 144106 (2017).
[57]T. Scholak and P. Brumer, Adv. Chem. Phys. **162**, 39 (2017).
[58]P. Hamm, M. Lim, and R. M. Hochstrasser, J. Phys. Chem. B **102**, 6123 (1998).
[59]L. Ackels, P. Stawski, K. E. Amunson, and J. Kubelka, Vib. Spectrosc. **50**, 2 (2009).
[60]N. Grnbech-Jensen and O. Farago, Mol. Phys. **111**, 983 (2013).
[61]C. Loken, D. Gruner, L. Groer, R. Peltier, N. Bunn, M. Craig, T. Henriques, J. Dempsey, C.-H. Yu, J. Chen, L. J. Dursi, J. Chong, S. Northrup, J. Pinto, N. Knecht, and R. V. Zon, J. Phys.: Conf. Ser. **256**, 012026 (2010).
[62]S. M. Gallagher Faeder and D. M. Jonas, Phys. Rev. A **62**, 033820 (2000).